

Investigation of Fatigue Growth Behavior of an Inclined Crack in Aluminum Alloy Plate

Jun Wang · Xing-Quan Zhang · Wei Wei · Jin-Yu Tong ·
Bin Chen · Guang-Wu Fang · Yuan-De Yin

Submitted: 18 March 2018 / in revised form: 29 May 2018 / Published online: 2 July 2018
© ASM International 2018

Abstract In the present paper, fatigue tensile tests are carried out on a servo-hydraulic fatigue testing machine to study the whole propagation process of the inclined crack. And the scanning electron microscope is employed to observe the micromorphology of the fracture surface to further probe the crack growth rate from a microscopic point of view. Meanwhile, the finite element method has also been applied to predict the crack propagation trajectory and the fatigue life of the sample with two finite element analysis codes. The fatigue tensile tests indicate the inclined crack propagates along the direction perpendicular to the external loading and the crack growth rate increases continuously based on the micromorphology of the fracture surface. The numerical analysis results reveal the variation of the stress distribution at the crack tip as well as the crack trajectory at different extension steps. Moreover, the stress intensity factor values are discussed in detail. And the computed results, the inclined crack propagation path and fatigue life of the sample, agree well with the experimental ones, which provide certain referential significance for the prediction of the inclined crack propagation in thin plate.

Keywords Edge notched specimen · Tensile tests · Micromorphology · Numerical simulation · Fatigue life · SIF

Introduction

The crack generally is prone to initiate at the stress concentration areas where there exist the rivet holes, sharp V-notches that are simplified from complicated local geometric features, and so on [1–4]. The crack and its propagation can lead to the decrease in the structure strength and even result in catastrophe eventually. Consequently, it is of great necessity to acquire a better understanding of crack propagation behavior. And the historical origins for crack researches can be traced back to Griffith's pioneering work which makes crucial contributions to the fracture theory on the brittle material in 1920s [5]. Irwin proposed stress intensity factor (SIF) in 1957 and established crack propagation criteria based on the previous studies [6], which greatly facilitated the advancement of the fracture mechanics. And in the past few decades there have been many studies devoted to the cracks in mixed mode condition. The mixed mode fracture takes place when bi-/multi-axial stress state [7] or cracks that are non-perpendicular to loading direction exist in the sample. Shlyannikov investigated the fatigue crack paths for the inclined surface cracks and the surface flaws under the biaxial loading [8]. Slobodanka et al. examined the mixed mode crack propagation process for an Arcan and a single edge specimen using the proposed procedures under mixed mode conditions [1]. Benedetti et al. experimentally researched the influence of the notch geometry on the fatigue cracks propagation in sharp V-shaped notches and employed linear elastic fracture mechanics to analyze the experimental results [3].

In order to accurately forecast the crack growth rate, several crack propagation laws have been proposed. In 1963, Paris growth rate model was put forward based on

J. Wang · X.-Q. Zhang (✉) · W. Wei · J.-Y. Tong · B. Chen ·
G.-W. Fang · Y.-D. Yin
School of Mechanical Engineering, Anhui University of
Technology, Ma'anshan 243002, China
e-mail: zhang20020313@163.com

J. Wang
e-mail: 201225040412@chd.edu.cn

the fracture mechanics, which described a simple power-law relationship between the crack growth rate and SIF [9]. Later, R ratio was introduced into Paris model and the Walker growth model was established [10]. Nevertheless, both of them are insensitive to the near-threshold and near-critical region. Accordingly, other modified equations including coefficients such as the fracture and stress ratio simultaneously were presented in succession [11]. Furthermore, new methods like two-parameter driving force model combined with the equivalent SIF have been used to calculate the fatigue life of the components in recent years [1, 2]. Hu et al. posed a new enriched finite element method to study the fatigue crack growth [12] and pointed out the fatigue life could be calculated after the corresponding equivalent SIF exceeded the material fracture toughness, which signified the initiation of the crack instability propagation. Similarly, such failure criterion was also adopted in predicting the fatigue crack growth in compressor blade [13], cracked gear tooth [14], etc.

The aim of the paper is to probe the possibility of simulating growth process of the inclined crack in a single edge inclined notched (SEIN) specimen with the codes ABAQUS 6.14 and FRANC3D V6.0. The fatigue tests are carried out, and the micromorphology of the specimen fracture surface after the experiments is detected to evaluate the crack growth rate at different stages. Moreover, the predictions of the propagation trajectory and fatigue life of the cracked SEIN specimen have been implemented via numerical analysis method and are compared with the experimental results. This study enables one to further understand the process of the crack propagation in aerospace aluminum alloy components with edge notch.

Experiments

Experimental Conditions

The material 7075-T6, a high-strength and low-density aluminum alloy, was selected due to its wide application in aerospace manufacturing field, and the chemical composition of the material (wt.%) consists of 0.04Ti, 0.19Cr, 0.10Si, 0.25Fe, 0.09Mn, 2.55Mg and 1.76Cu. The brick SEIN sample was 100 mm long, 60 mm high and 2 mm thick, which was fabricated employing wire electrical discharge machining (WEDM) from the commercial product of 7075-T6 aluminum alloy sheet. An inclined notch located at 45° angle with respect to the loading direction and a pre-crack with 5 mm length at the tip of notch were also fabricated by WEDM. And after cutting, the SiC sandpapers with grain size of 1200 were adopted for wiping off the burrs at the edges.

Subsequently, the fatigue tensile tests were conducted on a servo-hydraulic fatigue testing machine with a loading

capacity of 100 kN/500 Nm at room temperature. Two ends of the SEIN specimen were, respectively, clamped by the top and bottom fixtures, as shown in Fig. 1. The cyclic load with maximum value of 5 kN and load ratio of 0 was loaded on the SEIN specimen, and the frequency was 8 Hz. The fatigue test information incorporating the dynamic loading curve, real-time displacement as well as the loading cycle numbers was documented during the experiments, and the crack trajectory was also recorded by an industrial camera at a certain time interval.

Test Results

After a long time of tensile fatigue test, the SEIN specimen is broken into two pieces. The broken sample and its fracture surface are presented in Fig. 2. Along the crack propagation direction, the fracture surface can be divided into the larger smooth area, the smaller rough area and the last necked rupture area which possesses a characteristic of fatigue failure. Therefore, the propagation process of the pre-fabricated crack can be segmented into three stages, namely the stable crack growth stage, the unstable rapid crack growth stage and the abrupt fracture stage.

To observe the micromorphology of the fracture surface explicitly, SEM with voltage 5 kV was employed and seven typical regions shown in Fig. 2 were selected and detected to reflect the rate of crack growth.

Figure 3 depicts the surface micromorphology of the crack pre-fabricated by WEDM located at region 1 in Fig. 2. As shown in picture, there exist numbers of craters and globular particles on the machined surface. As is well known, the electrical discharge between the wire and sample



Fig. 1 Fatigue tensile experiments

Fig. 2 Fractured sample and micromorphology of the fracture surface

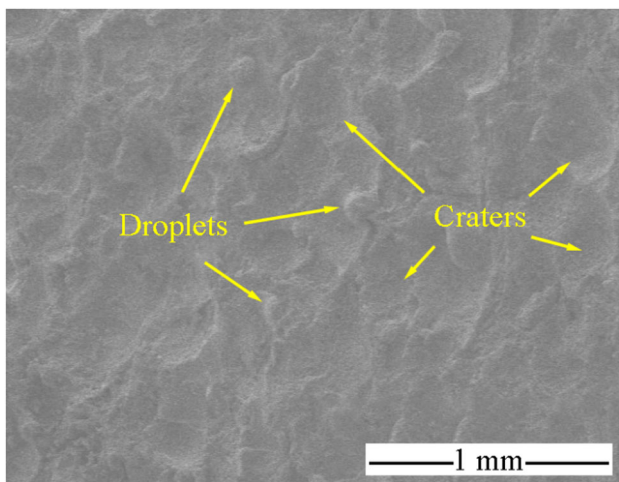
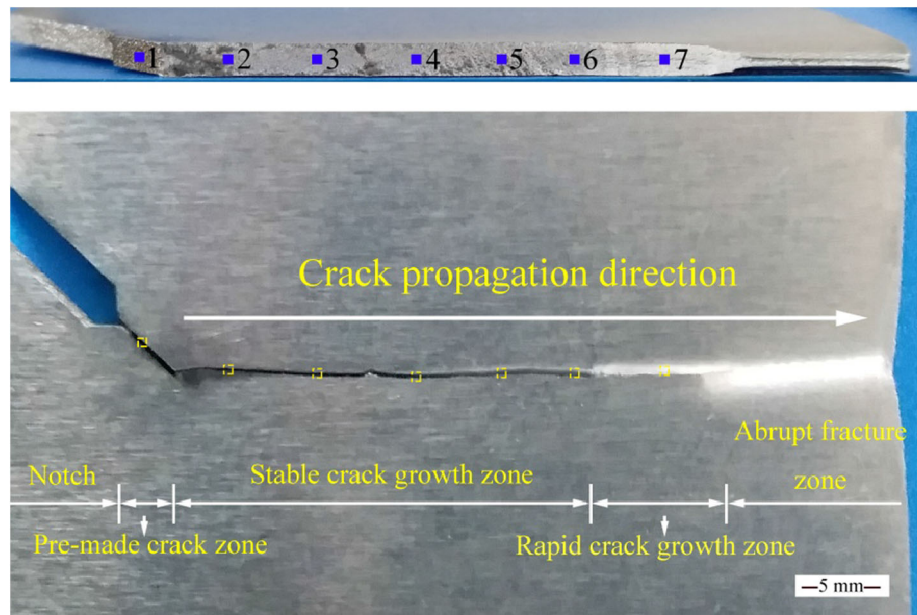


Fig. 3 Surface micromorphology of the crack pre-fabricated by WEDM

causes the transient high temperature, which melts the material around the wire, even vaporizes a small portion of the metal material. Meanwhile, the high temperature also leads to the vaporization of a part of the operating fluid flowing in the electrical discharge zone during the machining process of WEDM. The vaporized material and operating fluid expand instantly and form the micro-explosion. The shock wave of explosion generates a high pressure on the heated soft surface, tossing the melt material from the matrix and forming craters. And the melt material adhered to the surface exists as droplets eventually after cooling.

Figure 4a, b, c, d, e and f display the micromorphologies of the regions 2–7 in Fig. 2, respectively. In Fig. 4a and b,

numerous rugged crystallographic facets and river-like patterns can be observed clearly, which indicate that the crack propagates along different crystallographic facets. At this time, due to extremely slow propagation of the crack, the fatigue striations cannot be viewed even at a high magnification. With the propagation of the crack, the ripple-like parallel fatigue striations can be seen in Fig. 4c, d and e. The fatigue striations are perpendicular to the crack growth direction, and the spacing between them corresponds to the crack propagation distance per cycle during fatigue test [15]. From Fig. 4c, d and e, it can be computed that the average spacing of the fatigue striations is about 3.1, 4.4 and 5.6 $\mu\text{m}/\text{cycle}$, respectively. The fatigue striations are getting wider and wider, which indicates the crack growth rate is increasing continuously. And when the crack growth enters into the unstable crack propagation stage, the parallel fatigue striations disappear and the dimples exist on fracture surface, as displayed in Fig. 4f, which result from the formation and rapid growth of the micro-voids in the vicinity of the defects in material. The inclusion particles can also be observed in the figure, and they can accelerate the crack propagation. Consequently, the crack growth rate increases promptly at this stage. During the crack growth process, the relation of the crack growth length with the cycle numbers is plotted in Fig. 5, which also verifies the crack growth rate continues to increase.

Numerical Simulation

A coupled use of ABAQUS 6.14 and FRANC3D V6.0 software has been implemented in numerical simulation

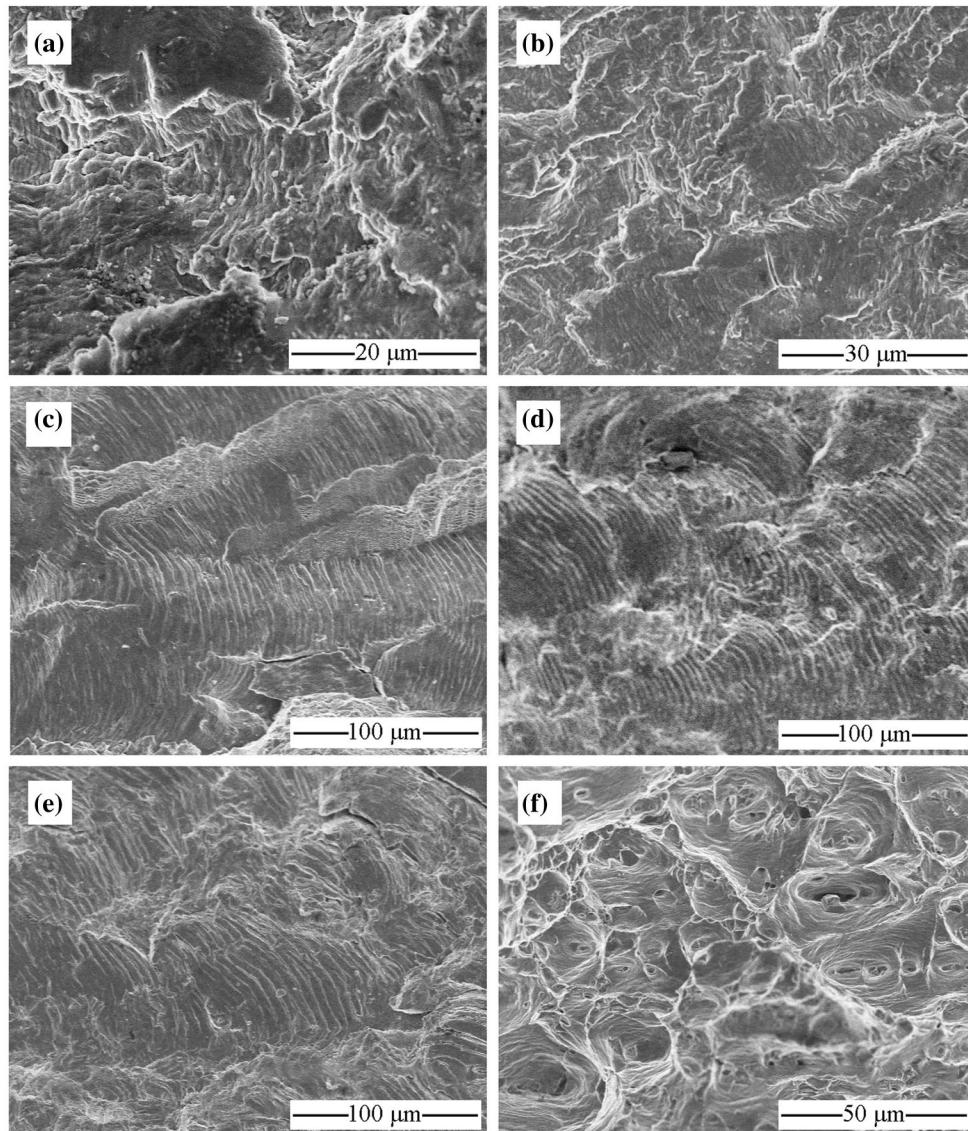


Fig. 4 Micromorphologies of the fracture surface at different stages (a)–(f) correspond to the regions 2–7 in Fig. 2

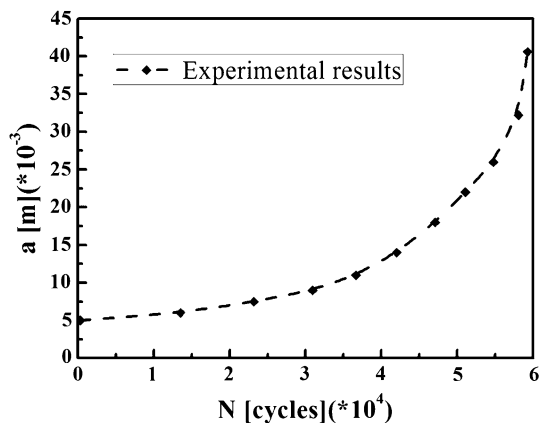


Fig. 5 Crack propagation length at different loading cycles

process. ABAQUS 6.14, a set of engineering analysis software, is developed by the HKS company in the USA. It has two main solver modules ABAQUS/Standard and ABAQUS/Explicit. For the former one, ABAQUS/Standard is a general analysis module, which can solve various linear and nonlinear complicated problems. And ABAQUS/Explicit module is suitable for analyzing the transient dynamic problems such as laser shocking and explosions. In this paper, ABAQUS/Standard module is employed to establish the initial model and to analyze the stress field in current case. FRANC3D V6.0 (FRacture ANalysis Code for 3D/version 6.0) is a new-generation crack analysis software developed by FAC (Fracture Analysis Consultants, Inc.) in the USA. And it allows one to define initial

cracks inserted into the finite element model, which depends on the finite element analysis code to analyze the cracked model and utilizes the above analytical results to calculate the SIF values [16].

Finite Element Model

According to the size of the mentioned above-tested specimen, a finite element model was established with the code ABAQUS 6.14. The material mechanical property parameters, the elastic modulus 71.7 GPa, Poisson’s ratio 0.3 and the fracture toughness 938.25 MPa·mm^{1/2}, were used to describe the mechanical behavior. The element with eight-node hexahedral linear reduced integration was adopted to mesh the established model. A linear loading with 0.083 kN/mm was loaded upon its one end, and the displacement constraint was applied at the other end, as shown in Fig. 6.

Fatigue Crack Propagation Model

The Paris equation has been widely used to estimate the crack growth rate in the past, which proves effective only to the linear stable crack propagation region. Another crack

growth rate equation, NASGRO model, is effective to the whole region of the crack propagation curve [17]. The NASGRO model takes into consideration the *R* ratio and the influence of crack opening effect on the crack growth rate, which is more intricate than the Paris equation. It can be written as [18]:

$$\frac{da}{dN} = C \left(\frac{1-f}{1-R} \Delta K \right)^n \frac{\left(1 - \frac{\Delta K_{th}}{\Delta K} \right)^p}{\left(1 - \frac{K_{max}}{K_c} \right)^q}, \tag{Eq 1}$$

where *a* represents the crack length, *N* is the loading cycle number, *da/dN* denotes the crack growth rate, and *C* and *n* are empirical data, which resemble those describing the curve’s linear region in Paris model. Exponents *p* and *q* signify empirical coefficients illustrating the curvature of the near-threshold and near-critical region of the crack propagation rate model. *R* is the stress ratio; parameter *f*, a function about the crack opening, is expressed in Ref. [14]. *K_c* relevant to the materials’ fracture toughness expresses the critical value of the SIF. *K_{max}* is the maximum value of the SIF. ΔK is the SIF range, which mainly depends on the applied loading, and its value relies on the difference between the values of the maximum and the minimum SIF. ΔK_{th} , the threshold SIF range, defines a value from which the crack extension initiates, viz. crack will cease to propagate below the value. These applied sixteen fitting parameters in this equation can be selected from the database of the program if the material is determined.

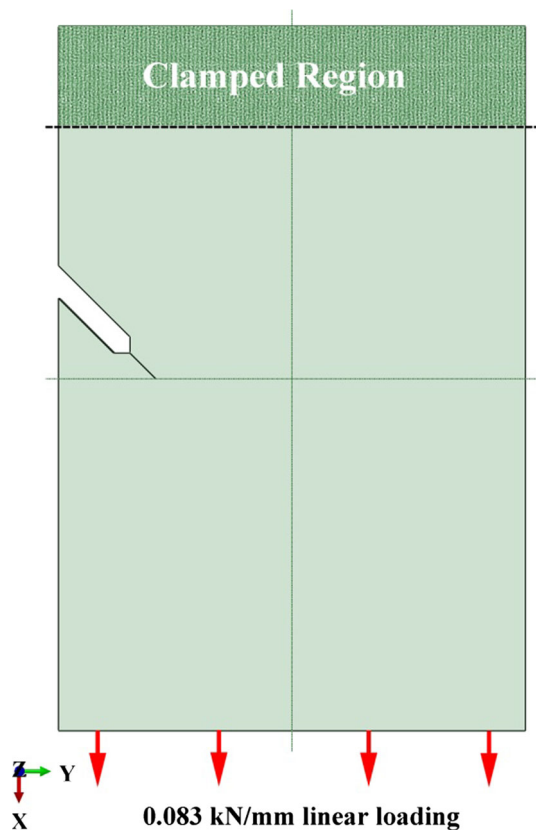


Fig. 6 Geometry of the finite element model

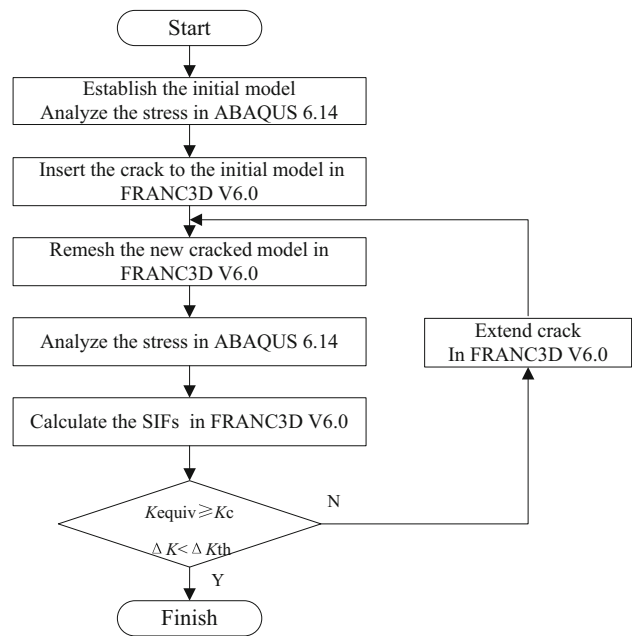


Fig. 7 Flowchart of crack propagation simulation

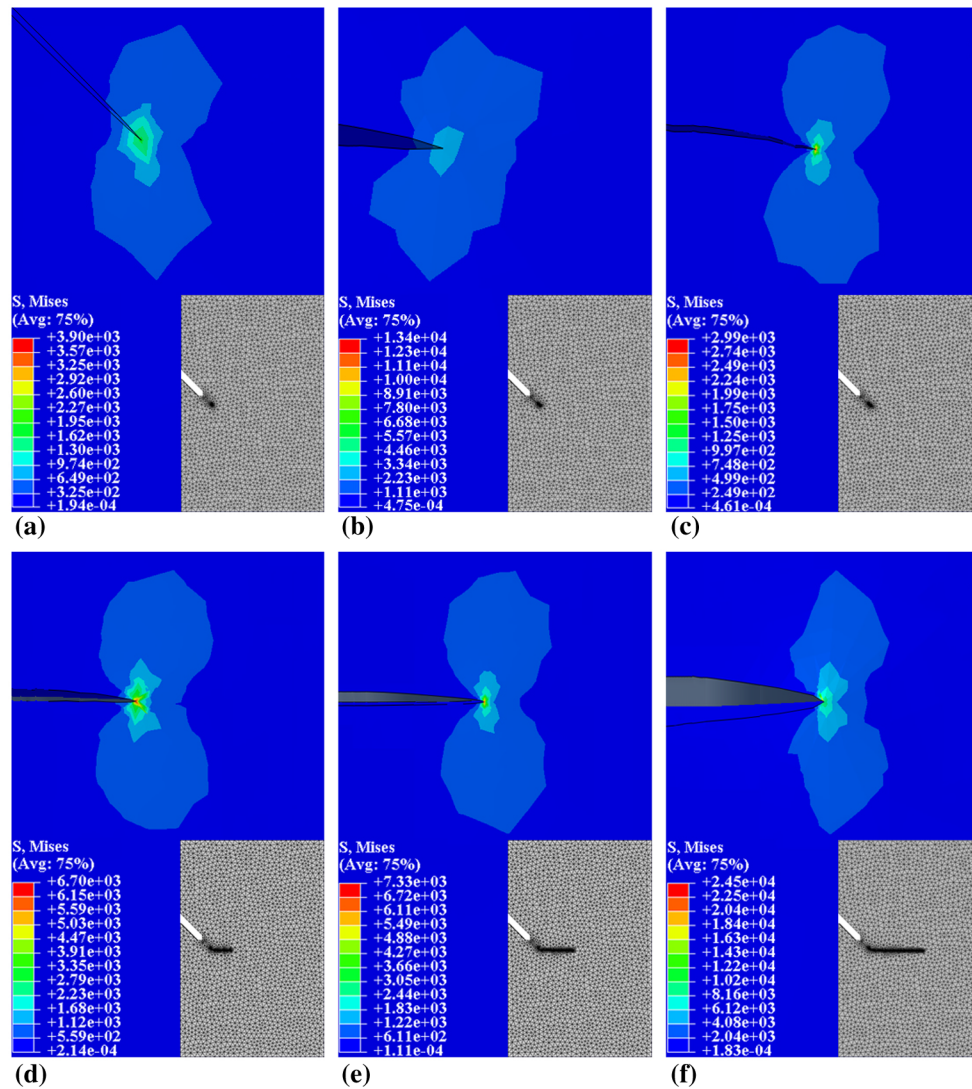


Fig. 8 Stress distribution around the crack tip as well as the predicted crack propagation trajectory extracted from ABAQUS 6.14 (2 times magnification for its displacement). (a) Analytical result, (b) 1st step, (c) 2nd step, (d) 20th step, (e) 40th step, (f) 60th step

Flowchart of the Numerical Simulation

As mentioned above, two codes ABAQUS 6.14 and FRANC3D V6.0 are employed to simulate the crack growth. Initially, the finite element model is developed and analyzed in ABAQUS 6.14 software. Then the analytical result is imported into FRANC3D V6.0 to implement the insertion of the corner crack and remeshing of the cracked model. Afterward, the stress analysis is executed based on the built-in program in code ABAQUS 6.14 for calculating the SIFs of the crack front. K_{equiv} , equivalent SIF, is

$$K_{\text{equiv}} = \frac{K_I}{2} + \frac{1}{2} \sqrt{K_I^2 + 4(1.155K_{II})^2 + 4K_{III}^2}, \quad (\text{Eq } 2)$$

where K_I , K_{II} and K_{III} are the SIFs for mode I, mode II and mode III, respectively. K_{equiv} is used to compare with the fracture toughness of the material K_C . When K_{equiv} is greater than or equal to K_C , the crack growth will enter into the unstable rapid crack growth stage [17]. The process of simulation is shown in Fig. 7.

Computing Results

After a series of calculations according to the flowchart shown in Fig. 7, the stress distribution at the crack tip, crack propagation trajectory as well as the crack growth rate can be obtained.

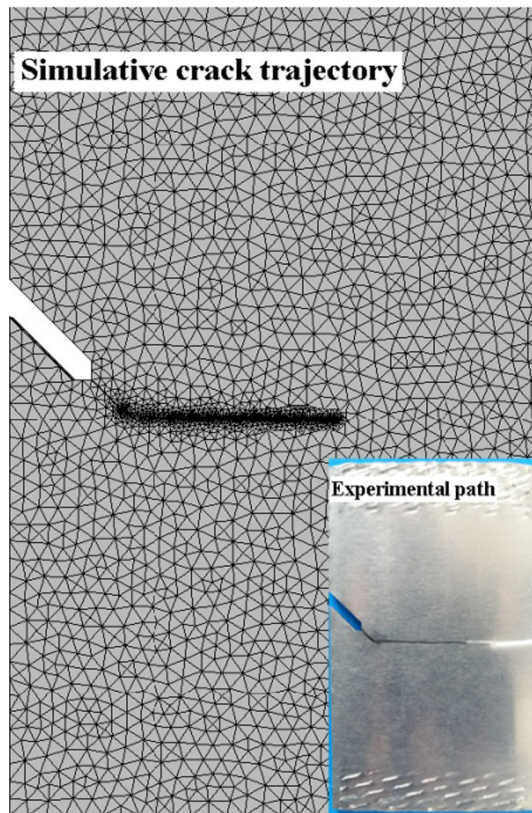


Fig. 9 Description of the crack propagation trajectory

Stress Distribution and Crack Propagation Trajectory

Figure 8 depicts the stress distribution around the crack tip at different crack extension steps. As presented in Fig. 8a and b, the stress field at the crack tip is asymmetric at the initial stage, and it turns to be symmetrically distributed along the crack propagation direction with the added crack extension steps, as displayed in Fig. 8c, d, e and f. It can be concluded that the crack growth direction has changed in accordance with the variation of the stress field at the crack tip. Furthermore, the meshes of the model at the corresponding extension steps are also shown in Fig. 8.

Figure 9 depicts the whole crack propagation trajectory, from which it can be obviously seen that the crack does not grow along the direction of the initial pre-fabricated inclined crack and the growth direction alters. The crack almost propagates along a straight line which is perpendicular to the direction of applied load. Additionally, the experimental crack path that is almost a line under the same conditions is also demonstrated in Fig. 9. The correctness of the numerical analysis can be well verified.

SIFs at the Crack Front

The SIF, an essential factor to judge the process of the crack propagation, deserves further analysis. In the current case, the SIF values for K_I , K_{II} and K_{III} can be figured out from FRANC3D V6.0. Figure 10 displays the calculated results of the SIF values at four stages. As shown in Fig. 10a, SIF values of modes I, II and III are, respectively, presented. The value of K_I ranges from 275 to 300 $\text{MPa}\cdot\text{mm}^{1/2}$ and K_{II} changes slightly around $-140 \text{ MPa}\cdot\text{mm}^{1/2}$, while K_{III} approaches 0. The results indicate the crack propagation belongs to mixed mode dominated by modes I and II at initial crack growth stage. And with the increase in extension distance, the SIF values of K_I increase, while K_{II} and K_{III} are almost constant, as shown in Fig. 10b, c and d. For example, at step 40, the maximum K_I is up to 709 $\text{MPa}\cdot\text{mm}^{1/2}$, while K_{II} and K_{III} are about zero. It indicates the mixed mode crack propagation turns into mode I in later crack growth stage due to the effect of external loading.

Figure 11 further displays the SIF values of K_I from step 66 to step 70 individually. And it can be seen that the K_I values at the crack front increase continuously. Due to dominant mode I, K_{equiv} is approximately equal to K_I in the calculation. At step 69, the maximum K_I of the crack front is about 936.20 $\text{MPa}\cdot\text{mm}^{1/2}$ which is close to the K_C (938.25 $\text{MPa}\cdot\text{mm}^{1/2}$) of the tested aluminum alloy. And at step 70, the maximum K_I reaches 944.90 $\text{MPa}\cdot\text{mm}^{1/2}$ and K_{equiv} is greater than K_C , which indicates the crack has entered into an unstable rapid growth stage.

Crack Growth Rate

Figure 12 reveals the relation of the crack growth length with the loading cycle numbers, and the corresponding experimental results are plotted together. As shown in the figure, a large similarity exists between two curves for the same overall trend.

At the crack initial growth stage, the crack grows slowly with the increasing cycle loading numbers. After the loading cycle numbers reach 48,790 in simulation, the crack growth rate rises obviously. And the crack subjected to 50,891 cycles enters into the unstable rapid crack stage with the predicted crack growth length 30.2 mm. In the experiment, when the SEIN specimen experiences 59,274 loading cycle numbers, the initial crack length grows to 35.6 mm and then the specimen breaks abruptly into two pieces. Compared with the experimental values of crack length and cycle numbers, the predicted values deviate by 15.2% and 14.1%, respectively, which verify the validity of the developed finite element model and further analysis.

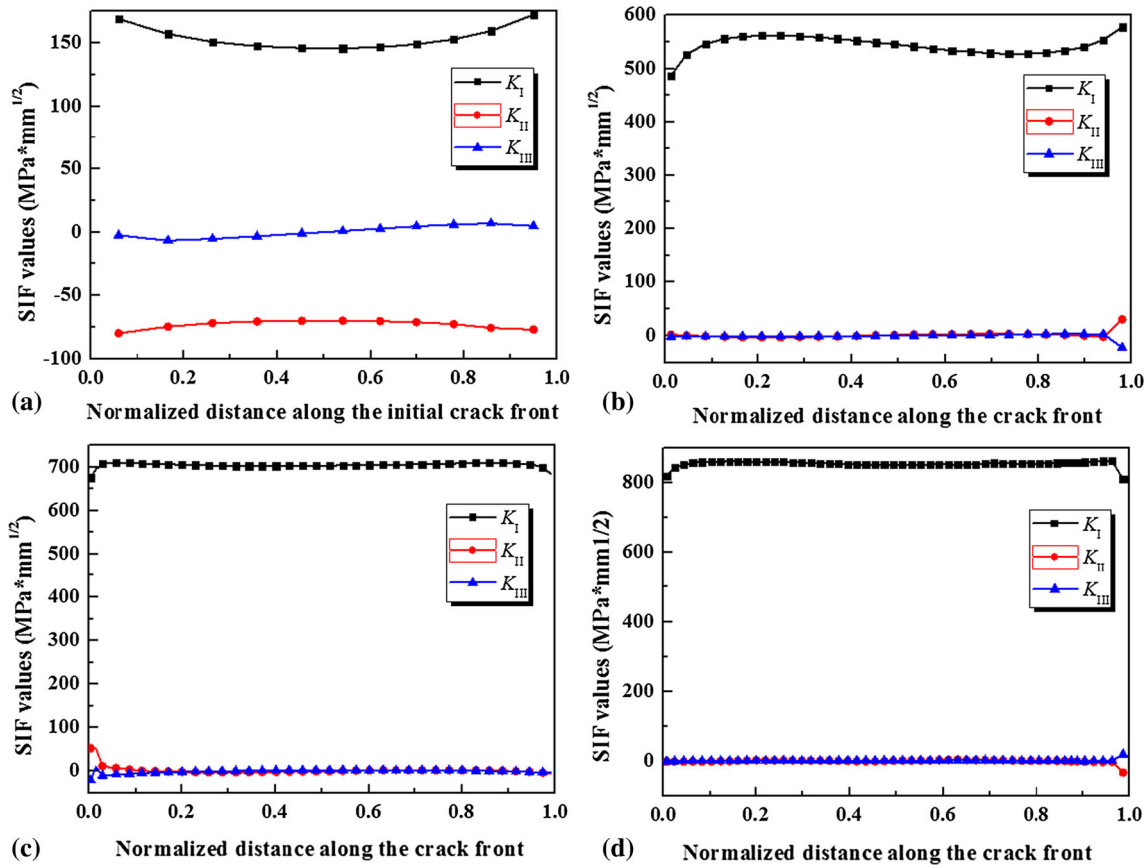


Fig. 10 SIF values of the crack front at different extension steps: (a) 1st step, (b) 20th step, (c) 40th step, (d) 60th step

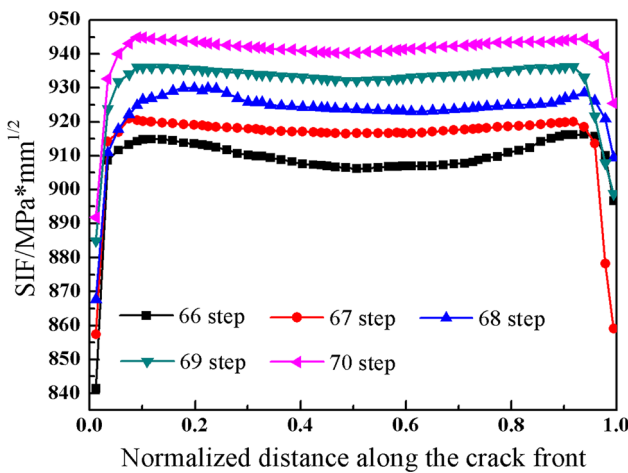


Fig. 11 SIF values from the 66th to 70th extension steps

Conclusion

The process of the inclined crack propagation in a SEIN specimen has been investigated by experiments and the finite element method. Under the external cycle loading, the crack propagation mode alters from mixed mode I/II in

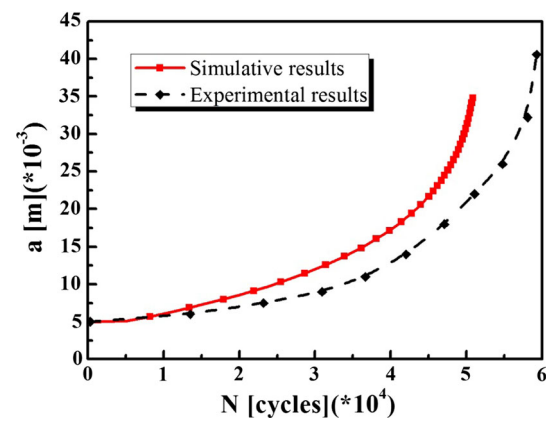


Fig. 12 Relation of the crack length with the loading cycle numbers

initial stage to mode I, and the crack propagates faster and faster while fatigue striations become wider and wider. Finite element method can be applied to predict the fatigue crack growth path and rate, which can provide an example for the analysis of the mixed mode crack propagation problem with ABAQUS 6.14 and FRANC3D V6.0 software.

Acknowledgments The work was sponsored by the National Natural Science Foundation of China (Nos. 51675002, 51175002), National Natural Science Foundation of Anhui Province (No. 1708085ME110), Natural Science Foundation of Colleges and Universities in Anhui Province (Nos. KJ2016A813, KJ2016A806) and the Graduate Innovation Research Foundation of Anhui University of Technology (No. 2016073).

References

1. S. Boljanović, S. Maksimović, Mixed mode crack growth simulation with/without overloads. *Int. J. Fatigue* **67**, 183–190 (2014)
2. S. Boljanović, S. Maksimović, Computational mixed mode failure analysis under fatigue loadings with constant amplitude and overload. *Eng. Fract. Mech.* **174**, 168–179 (2017)
3. M. Benedetti, M. Beghini, V. Fontanari, B. Monelli, Fatigue cracks emanating from sharp notches in high-strength aluminum alloys: the effect of loading direction, kinking, notch geometry and microstructure. *Int. J. Fatigue* **31**, 1996–2005 (2009)
4. H. Alihosseini, K. Dehghani, Modeling and failure analysis of a broken railway axle: effects of surface defects and inclusions. *J. Fail. Anal. Prev.* **10**, 233–239 (2010)
5. A.A. Griffith, The phenomena of rupture and flow in solids. *Philos. Trans. R. Soc. Lond. A* **221**, 163–198 (1921)
6. G.R. Irwin, Fracture dynamics, in *Fracturing of metals seminar* (American Society for Metals, Cleveland, 1948), pp. 147–166
7. G. Fu, W. Yang, C.Q. Li, Stress intensity factors for mixed mode fracture induced by inclined cracks in pipes under axial tension and bending. *Theor. Appl. Fract. Mech.* **89**, 100–109 (2017)
8. V.N. Shlyannikov, Fatigue crack paths for inclined cracks and surface flaws under biaxial loading. *Eng. Fract. Mech.* **77**, 1772–1780 (2010)
9. W. Zhang, H. Liu, Q. Wang, J. He, A fatigue life prediction method based on strain intensity factor. *Materials* **10**, 689 (2017)
10. I.S. Raju, J.C. Newman Jr., Three dimensional finite-element analysis of finite-thickness fracture specimens. Report, NASA TN D-8414 (1977)
11. T. Sang, D. Kim, A. Tadjiev, T. Yang Hyun, Fatigue life prediction under random loading conditions in 7475-T7351 aluminum alloy using the RMS model. *Int. J. Damage Mech.* **15**, 89–102 (2006)
12. X.F. Hu, W.A. Yao, A new enriched finite element for crack growth. *Int. J. Fatigue* **48**, 247–256 (2013)
13. E. Poursaeidi, H. Bakhtiari, Fatigue crack growth in a first stage of compressor blade. *Eng. Fail. Anal.* **45**, 314–325 (2014)
14. X. Zhang, L. Li, X. Qi, J. Zheng, X. Zhang, Experimental and numerical investigation of fatigue crack growth in the cracked gear tooth. *Fatigue Fract. Eng. M* **40**, 1037–1047 (2017)
15. S. Huang, J.Z. Zhou, J. Sheng, K.Y. Luo, J.Z. Lu, Effects of laser peening with different coverage areas on fatigue crack growth properties of 6061-T6 aluminum alloy. *Int. J. Fatigue* **47**, 292–299 (2013)
16. S.B. Narasimhachary, K.S. Bhachu, S.R. Shinde, P.W. Gravett, J.C. Newman, A single edge notch specimen for fatigue, creep-fatigue and thermo-mechanical fatigue crack growth testing. *Eng. Fract. Mech.* (2017). <https://doi.org/10.1016/j.engfracmech.2017.08.011>
17. R.S. Christopher, Uncertainty quantification in crack growth modeling under multi-axial variable amplitude loading, Doctor's Thesis, Vanderbilt University, Nashville, 2010
18. NASA, Fatigue crack growth computer program NASGRO version 3.0-Reference manual, JSC-22267B, Lyndon B. Johnson Space Center, Texas (2000)